Journal of Zhejiang University-SCIENCE A (Applied Physics & Engineering) 2022 23(1):1-13
www.jzus.zju.edu.cn; www.springer.com/journal/11582
E-mail: jzus_a@zju.edu.cn

Research Article

https://doi.org/10.1631/jzus.A2100214

A design constraint for a double-acting telescopic hydraulic cylinder in a hydraulic erecting system

Xiao-long ZHANG[1], Jun-hui ZHANG[1], Min CHENG[2]✉, Shen ZHENG[1], Bing XU[1], Yu FANG[1]

[1]*State Key Laboratory of Fluid Power & Mechatronic Systems, Zhejiang University, Hangzhou 310027, China*
[2]*State Key Laboratory of Mechanical Transmissions, Chongqing University, Chongqing 400044, China*

Abstract: Hydraulic erecting systems are widely used in missile and rocket launchers because of their high power density. The double-acting telescopic hydraulic cylinder (DATHC) plays a decisive role in the safe and proper operation of such systems. In particular, improper design of effective areas of a DATHC could potentially lead to an overspeed descent with severe damage for the erecting system. Unfortunately, there is no design constraint for DATHC to prevent this. Therefore, in this paper, a simplified and practical design constraint is proposed. Based on a developed mathematical model of a typical erecting system, we simulated and analyzed not only six cases meeting and not meeting the design constraint, but also the effectiveness of the design constraint under different loads. Experiments were then carried out under four cases. Simulation and experimental results validate the simplified design constraint, a constraint inequation guiding the design of diameters of effective areas for a DATHC.

Key words: Erecting system; Telescopic hydraulic cylinder; Overspeed descent; Design constraint

1 Introduction

Hydraulic erecting systems, which are used to raise or lower an erecting beam from one angle position to another, are widely used in missile vehicles, large construction machinery, and other mechanical devices (Yang et al., 2019). Due to the requirement for a long stroke in a limited mounting space, a telescopic hydraulic cylinder, also called a multistage hydraulic cylinder, is routinely adopted in such systems (Gao, 2004). It is designed as a nested structure with gradually smaller diameters fitting within each other. The most prominent feature of a telescopic cylinder is its ability to provide an extremely long working stroke from a very compact retracted dimension. Telescopic cylinders can be divided into two types: single-acting and double-acting. Retraction of a single-acting telescopic cylinder relies only on gravity or an external force when the pressure is released from the piston chamber. In contrast, a double-acting telescopic hydraulic cylinder (DATHC) with two oil supply ports is powered hydraulically in both directions. Accordingly, a DATHC is more complex in design. As a critical component of a hydraulic erecting system, there are multifaceted considerations for the design of a DATHC to ensure the reliability of the erecting system, such as strength, stability, and size of effective areas at all stages.

There have been many studies of the strength of a DATHC when it is fully extended. Prakash et al. (2020) proposed a method to determine the safe load of a two-stage pin-mounted hydraulic cylinder. The results obtained by this method were in good agreement with finite element simulation results. Uzny and Kutrowski (2019) investigated the influence of mounting rigidity on the strength of a telescopic hydraulic cylinder based on the static stability criterion. Their results showed that the buckling capacity increased when the installation stiffness was increased. Wang et al. (2013) analyzed the stress and buckling behavior of a telescopic hydraulic prop under alignment load and eccentric load by finite element simulation. The results showed that a 360-type doubly-telescopic structure could withstand 1.1 times the eccentric load under the

✉ Min CHENG, chengmin@cqu.edu.cn
Xiao-long ZHANG, https://orcid.org/0000-0003-3368-1212
Min CHENG, https://orcid.org/0000-0002-8345-6657

Received May 8, 2021; Revision accepted Aug. 3, 2021;
Crosschecked Dec. 17, 2021

condition of full extension. Gupta et al. (2020) used the successive approximation method to determine the critical load of a two-stage hydraulic cylinder hinged at both ends, and the deviation was 3.63%. Li et al. (2015) put forward a dichotomous iterative method based on Python, through which the extreme load of a two-stage hoisting hydraulic cylinder can be quickly obtained.

To ensure the stability of a telescopic hydraulic cylinder during operation, Lgritskaia et al. (2021) adopted two telescopic hydraulics with different installation angles to reduce the pressure impact during the switching stages in launch vehicles. Due to different installation angles, the switching times of the two telescopic hydraulic cylinders were different: when one cylinder switched the stage, the other worked. In this way, the aim of reducing the pressure impact was achieved. Xie et al. (2014) established a mathematical model of a sizeable erecting system and designed a time-varying sliding mode controller whose performance was better than proportion integration differentiation (PID), according to the experimental results. However, the hydraulic actuator of this erecting system was not a DATHC. Several other papers have been devoted to the modeling and simulation of similar systems. Ritelli and Vacca (2013) developed a mathematical model of the counterbalance valve and analyzed the influence of its setting parameters on the energy consumption of a hydraulic crane system by a graphic method. Bak and Hansen (2013) optimized the operational reliability for an offshore material handling application, considering the instability of a pressure compensated directional control valve and a counterbalance valve. Zhou et al. (2012) and Hou et al. (2017) proposed a simulation model of a hydraulic lifting system with a proportional directional valve, which was used to study whether a novel valve compensation strategy was effective. To simplify the model of a double variable load sensing system in an excavator, Lin et al. (2021) ignored the effect of the safety valve, check valve, and pipelines. Cheng et al. (2017) developed a mathematical model for a typical electro-hydraulic system, which was used to investigate the dynamic characteristics of a proposed valve compensation controller.

However, there have been few studies concerning the size of effective areas at all stages. If these areas are not properly designed, it will probably lead to overspeed descent, resulting in severe system damage and economic losses. Hence, there is an urgent need to develop a DATHC design constraint limiting its effective areas to prevent overspeed descent. Additionally, to avoid unexpected and destructive accidents, it is worth building a simulation model to prove the reliability of the design constraint before experimenting. Although the systems studied above were different from the erecting system, they provided references for the modeling in this paper.

To avoid overspeed descent and ensure the operational reliability of an erecting system, we derive a practical design constraint for a DATHC, which is effective even if there is a switch between overrunning load and passive load during operation. Then, a simulation model of a typical erecting system is established, by which preliminary verification of the effectiveness of the design constraint can be achieved. Subsequently, the experimental platform is described, and results of the verification experiment are given. Finally, the mechanism of the overspeed descent caused by failure to satisfy the design constraint is further discussed, based on the simulation results.

2 Design constraint of DATHC

2.1 DATHC description

A schematic view of a DATHC, a two-stage hydraulic cylinder, is shown in Fig. 1. The first stage piston rod assembly (Stage 1), composed of piston 1 and piston rod 1, is nested in the barrel. Its piston chamber and piston rod chamber are represented by Chamber 1 and Chamber 2, respectively. Stage 1 is regarded as the cylinder tube of the second stage piston rod assembly (Stage 2) containing piston 2 and piston rod 2. Similarly, Chamber 3 and Chamber 4 respectively denote its piston chamber and piston rod chamber. Oil is able to flow between Chamber 1 and

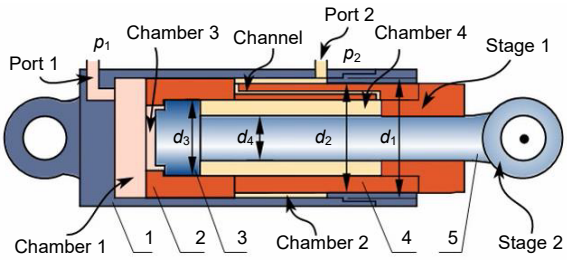

Fig. 1 Schematic view of a DATHC. 1: barrel; 2: piston 1; 3: piston 2; 4: piston rod 1; 5: piston rod 2

Chamber 3 with pressure p_1, whereas Chamber 2 and Chamber 4 with pressure p_2 are connected through a channel in piston rod 1. In Fig. 1, d_1, d_2, d_3, and d_4 are the corresponding diameters of the pistons and piston rods. When hydraulic oil is pumped into Chamber 1 and Chamber 3, Stage 1 extends with Stage 2. At the same time, the left end of Stage 2 is subjected to pushing force from Stage 1. Once Stage 1 is fully extended, the extension of Stage 2 relative to Stage 1 begins. With the movement of Stage 2, the oil in Chamber 4 is discharged to Chamber 2 via the internal channel in piston rod 1. As expected, the process of retraction is simply the reverse, and the port with pressure p_2 is the inlet in this case.

2.2 Derivation of design constraint

An external force can change the state of motion of a body. Therefore, to ensure the DATHC extends or retracts without an overspeed descent fault, it is necessary to carry out force analysis for Stage 1 and Stage 2.

According to the schematic diagram of forces acting on Stage 2 (Fig. 2), the force-balance equation is given by:

$$p_1 S_3 + f_{12} + F_{12} + F_{a2} = p_2 S_4 + F_{g2} + F, \tag{1}$$

where F is the external load of the DATHC and F_{a2} is the inertial force of Stage 2. The component force of gravity of Stage 2 is denoted by F_{g2}. S_3 and S_4 are the corresponding working areas of piston 2, $S_3 = \pi d_3^2/4$, and $S_4 = \pi(d_3^2 - d_4^2)/4$. f_{12} denotes the friction force exerted on Stage 2 by Stage 1. F_{12} is the force applied by Stage 1 on piston 2, which is generated by axial contact and extrusion between Stage 1 and piston 2. Accordingly, F_{12} exists only if Stage 2 is fully extended or retracted relative to Stage 1.

The forces acting on Stage 1 are shown in Fig. 3. The force balance equation can be written as

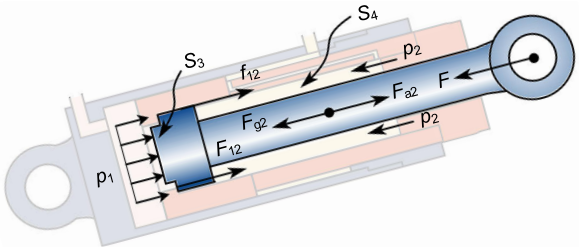

Fig. 2 Schematic diagram of forces acting on Stage 2. Variables are explained in the text

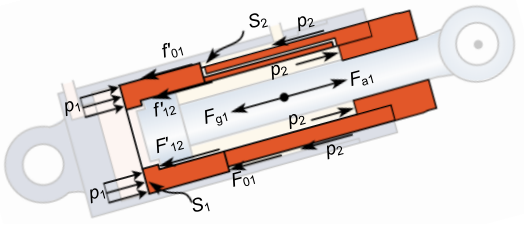

Fig. 3 Schematic diagram of forces acting on Stage 1

$$p_1 S_1 + p_2 S_4 + F_{a1} = p_2 S_2 + F'_{12} + f'_{12} + f_{01} + F_{01} + F_{g1}, \tag{2}$$

where S_1 and S_2 are the corresponding working areas of piston 1, $S_1 = \pi(d_1^2 - d_3^2)/4$, and $S_2 = \pi(d_1^2 - d_2^2)/4$. f_{01} is the friction force of the barrel against Stage 1. f'_{12} and F'_{12} are the reaction forces of f_{12} and F_{12}, respectively. F_{a1} denotes the inertial force of Stage 1. The component force of gravity of Stage 1 is expressed by F_{g1}. F_{01} is the force of the barrel against piston 1 due to axil extrusion.

The combination of Eqs. (1) and (2) leads to the following equation:

$$\begin{aligned} FS_1 = {} & p_2\left[S_2 S_3 - \left(S_1 + S_3\right) S_4\right] + \\ & \left(f_{01} + F_{01} + F_{g1} - F_{a1}\right) S_3 + \\ & \left(F_{12} + f_{12}\right)\left(S_1 + S_3\right) + \left(F_{a2} - F_{g2}\right) S_1. \end{aligned} \tag{3}$$

If Stage 1 is to extend first with Stage 2, F_{12} must exist and be greater than 0. In other words, hydraulic pressure alone cannot drive Stage 2 at this time. Moreover, F_{01}=0 is true because there is no axial contact between Stage 1 and the barrel. As a result, from Eq. (3), the constraint on the normal operation of DATHC can be obtained as follows:

$$\begin{aligned} FS_1 > {} & p_2\left[S_2 S_3 - (S_1 + S_3) S_4\right] + f_{12}\left(S_1 + S_3\right) + \\ & \left(f_{01} + F_{g1} - F_{a1}\right) S_3 + \left(F_{a2} - F_{g2}\right) S_1. \end{aligned} \tag{4}$$

Likewise, inequation (4) can also be obtained by analyzing the retraction process. However, p_2, F_{a1}, F_{a2}, F_{g1}, F_{g2}, f_{01}, and f_{12} are unknown until the design of the DATHC is completed, so inequation (4) cannot be used directly to determine the values of S_1, S_2, S_3, and S_4 in the design. Thus, it is necessary to simplify and modify the inequation to make it simple and easy to use. To accomplish this, some assumptions are proposed, as follows:

(a) Since the mass of each stage of the DATHC is much less than the sum of the mass of the erecting beam and load, the influence of F_{g1} and F_{g2} is not taken into account.

(b) As the acceleration of each stage in the smooth operation of the erecting system is slight, the inertial force is ignored.

(c) In practice, the directions of f_{01} and f_{12} change, but we merely consider an extreme case that is more likely to make inequation (4) untrue. That is, both f_{01} and f_{12} are positive, and $f_{01}=f_{12}=f$. It is assumed that f is very small and $2f<p_1S_1$ is satisfied.

The simplified inequation (4) can now be expressed as

$$F-f\left(1+\frac{2S_3}{S_1}\right)>\frac{p_2\left[S_2S_3-\left(S_1+S_3\right)S_4\right]}{S_1}. \tag{5}$$

Further, p_2 also can be substituted. Since $F_{12}\geqslant 0$ during the operation of the DATHC, we can conclude, according to Eq. (1) and the above hypotheses, that:

$$p_2\geqslant\frac{-F+f\left(1+\dfrac{2S_3}{S_1}\right)}{S_4}>0. \tag{6}$$

Next, we need to determine whether the right side of inequation (5) is positive. A schematic diagram of the $F-\varphi$ relationship is shown in Fig. 4. φ is the angle between the erecting beam and the horizontal plane. G is the gravitational force on the erecting beam and load. From point C to D, F is negative, which means that at least inequation (7) should be satisfied to make inequation (5) hold for any F.

$$S_2S_3-\left(S_1+S_3\right)S_4<0. \tag{7}$$

By substituting inequations (6) and (7) into inequation (5) and describing areas with diameters, a simplified and practical design constraint of a DATHC can be obtained:

$$\lambda<-1, \tag{8}$$

where λ is the structural parameter of the DATHC, defined as

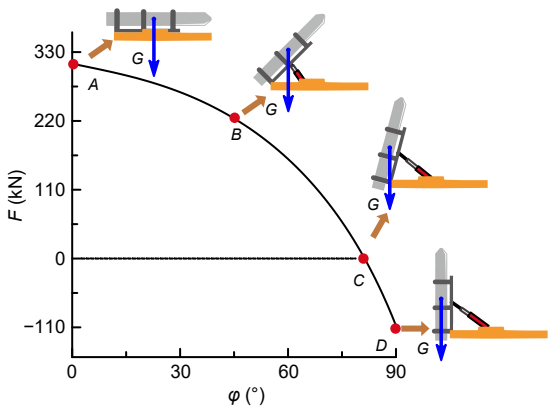

Fig. 4 Schematic diagram of F–φ relationship

$$\lambda=\frac{d_1^2d_4^2-d_2^2d_3^2}{\left(d_1^2-d_3^2\right)\left(d_3^2-d_4^2\right)}. \tag{9}$$

3 Modeling of hydraulic erecting system

A typical hydraulic erecting system is shown in Fig. 5. In this section, a simulation model is established to evaluate the feasibility of the proposed design constraint. In this way, the damage caused by direct and rash experimentation can be avoided. To simplify the model, the following assumptions were made:

(a) The influence of part compliance and fit clearance between them is ignored. Though they have a greater impact on system control accuracy, which is not the focus of this paper, they would have little influence on the research results of this study.

(b) At an operating pressure of 21 MPa, the deformation of the high-pressure hose (34.5 MPa) has little influence on the effective bulk modulus of the system, so it is ignored.

The leakage of the pump, which has a great influence on the flow rate of a hydraulic system, is considered, while the leakage of the valves is very limited by comparison and is ignored.

Given the effect of oil compressibility and leakage on the volumetric efficiency of the pump, the flow rate at the pump outlet can be expressed as (Park et al., 2020):

$$q_{\mathrm{p}}=\frac{Vn}{60}-\frac{V_{\mathrm{p}}}{\beta}\frac{\mathrm{d}p_{\mathrm{p}}}{\mathrm{d}t}-c_{\mathrm{p}}\Delta p_{\mathrm{p}}, \tag{10}$$

where V is the geometric displacement; n is the speed of the pump; V_{p} is the volume of the displacement

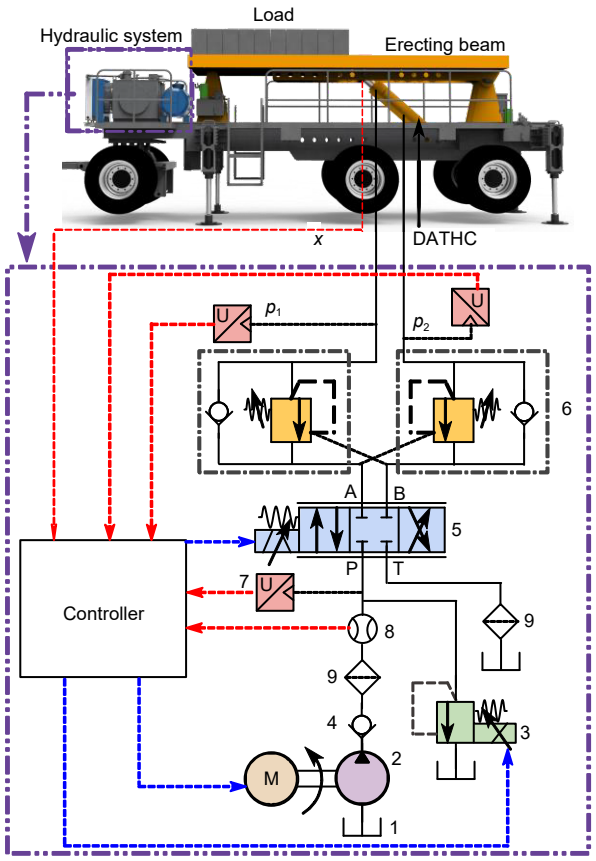

Fig. 5 Hydraulic erecting system. 1: oil tank; 2: pump; 3: pressure-relief valve (PRV); 4: check valve; 5: proportional directional control valve (PDCV); 6: counterbalance valve; 7: pressure sensor; 8: flow sensor; 9: filter. *x* is the displacement of the DATHC

chamber of the pump; β is the effective bulk modulus of the hydraulic fluid; t is the time; p_p, Δp_p, and c_p respectively denote the operating pressure, pressure difference of the pump, and coefficient of leakage, which is calculated by substituting the actual measured pressure difference and flow rate, as well as the displacement and rotational speed in the pump manual, into Eq. (10).

Ignoring the hysteretic behavior of the check valve, the flow rate across the check valve, whose flow rate-pressure drop characteristic is regarded as linear during the valve regulation, can be written as

$$\begin{cases} q_p = \Delta p_{c4} k_{c4}, & \Delta p_{c4} > 0, \\ q_p = 0, & \Delta p_{c4} \leqslant 0, \end{cases} \tag{11}$$

where $\Delta p_{c4}=p_p-p_s-p_{k4}$; p_s is the pressure between the check valve and the PDCV; p_{k4} and k_{c4} represent the check valve cracking pressure and flow rate pressure gradient, respectively.

Similarly, the flow rate of the PRV can be simplified and expressed as

$$\begin{cases} q_r = \Delta p_{r3} k_{r3} - \dfrac{V_r}{\beta} \dfrac{\mathrm{d}p_s}{\mathrm{d}t}, & \Delta p_{r3} > 0, \\ q_r = 0, & \Delta p_{r3} \leqslant 0, \end{cases} \tag{12}$$

where $\Delta p_{r3}=p_s-p_o-p_{k3}$; p_o is the pressure of the oil tank; p_{k3} and k_{r3} are the PRV cracking pressure and flow rate pressure gradient, respectively; V_r is the total volume of the connecting chamber between the check valve, PRV, and PDCV.

The flow-pressure characteristic of the ideal PDCV is described by

$$\begin{aligned} q_A &= C_d W_v x_d \sqrt{\frac{2 \cdot |\Delta p_A|}{\rho}} \operatorname{sign}(\Delta p_A), \\ \Delta p_A &= \begin{cases} p_s - p_A, & x_d > 0, \\ p_A - p_o, & x_d < 0, \end{cases} \end{aligned} \tag{13}$$

$$\begin{aligned} q_B &= C_d W_v x_d \sqrt{\frac{2 \cdot |\Delta p_B|}{\rho}} \operatorname{sign}(\Delta p_B), \\ \Delta p_B &= \begin{cases} p_B - p_o, & x_d > 0, \\ p_s - p_B, & x_d < 0, \end{cases} \end{aligned} \tag{14}$$

where x_d is the displacement of the spool, which is controlled by the input signal; q_A and q_B respectively denote flow rates in ports A and B, whose directions are determined by sign, a symbolic function; the pressures at ports A and B are indicated by p_A and p_B, respectively; C_d is the flow coefficient; W_v is the area gradient of the orifice; ρ is the oil density.

The counterbalance valve is composed of a main valve and a check valve. Consequently, the flow rate of the left counterbalance valve q_{cv1} can be written as

$$q_{cv1} = q_{m1} + q_{c1}, \tag{15}$$

where q_{m1} and q_{c1} denote the flow rates through the main valve and check valve, given by:

$$q_{m1} = C_m A_{mmax} \chi_{m1} \sqrt{\frac{2 \cdot |p_A - p_1|}{\rho}} \operatorname{sign}(p_A - p_1), \tag{16}$$

$$q_{c1}=C_c A_{cmax}\chi_{c1}\sqrt{\frac{2\cdot|p_A-p_1|}{\rho}}\operatorname{sign}(p_A-p_1), \quad (17)$$

where C_m, A_{mmax}, and χ_{m1} are the flow coefficient, maximum area, and fractional opening of the main valve, while the corresponding parameters of the check valve are represented by C_c, A_{cmax}, and χ_{c1}, respectively. χ_{m1} and χ_{c1} are calculated by:

$$\chi_{m1}=\frac{p_1+p_B\kappa-p_{mk}}{p_{mmax}-p_{mk}}, \quad 0\leqslant\chi_{m1}\leqslant 1, \quad (18)$$

$$\chi_{c1}=\frac{-p_1+p_A-p_{ck}}{p_{cmax}-p_{ck}}, \quad 0\leqslant\chi_{c1}\leqslant 1, \quad (19)$$

where κ is the pilot ratio; p_{mk} and p_{ck} are the cracking pressures of the main valve and check valve, respectively; p_{mmax} and p_{cmax} are the pressures for maximum opening of the main valve and check valve, respectively.

The relation between q_{cv1} and q_A is described as:

$$q_{cv1}=q_A-\frac{V_{cv1}}{\beta}\frac{\mathrm{d}p_A}{\mathrm{d}t}, \quad (20)$$

where V_{cv1} is the volume of the chamber between the left counterbalance valve and port A of the PDCV.

The flow rate of the right counterbalance valve q_{cv2} can be obtained following the same approach, and therefore is not shown here. For the DATHC, flow rates at port 1 and port 2 of the DATHC are expressed as:

$$q_{cv1}=\frac{\mathrm{d}x_1}{\mathrm{d}t}(S_1+S_3)+\left(\frac{\mathrm{d}x_2}{\mathrm{d}t}-\frac{\mathrm{d}x_1}{\mathrm{d}t}\right)S_3+\frac{V_1}{\beta}\frac{\mathrm{d}p_1}{\mathrm{d}t}, \quad (21)$$

$$V_1=x_1(S_1+S_3)+(x_2-x_1)S_3+V_{10}, \quad (22)$$

$$q_{cv2}=-\frac{\mathrm{d}x_1}{\mathrm{d}t}S_2-\left(\frac{\mathrm{d}x_2}{\mathrm{d}t}-\frac{\mathrm{d}x_1}{\mathrm{d}t}\right)S_4-\frac{V_2}{\beta}\frac{\mathrm{d}p_2}{\mathrm{d}t}, \quad (23)$$

$$V_1=-x_1S_2-(x_2-x_1)S_4+V_{20}, \quad (24)$$

$$x_{1max}\geqslant x_1\geqslant 0, \quad (25)$$

$$x_{2max}\geqslant x_2\geqslant 0, \quad (26)$$

where V_1 denotes the volume of current Chamber 1 and Chamber 3; V_2 denotes the volume of current Chamber 2 and Chamber 4; V_{10} is the sum of the dead volume and the volume of the chamber between the DATHC and the left counterbalance valve; V_{20} is the sum of the dead volume and the volume of the chamber between the DATHC and the right counterbalance valve; x_1 and x_2 are the displacements of Stage 1 and Stage 2 relative to the barrel, respectively; x_{1max} and x_{2max} are the maximums of x_1 and x_2, respectively.

The force balance equation of the DATHC was given in Section 2.1, as expressed in Eqs. (1) and (2). Nevertheless, there are some unknown variables that need to be further described.

Assuming that the stiction friction is equal to the Coulomb friction, and the Stribeck effect is not taken into account, one can obtain (Yanada and Sekikawa, 2008; Tran et al., 2012):

$$f_{01}=F_{coul1}+k_{f1}\frac{\mathrm{d}x_1}{\mathrm{d}t}, \quad (27)$$

$$f_{12}=F_{coul2}+k_{f2}\left(\frac{\mathrm{d}x_1}{\mathrm{d}t}-\frac{\mathrm{d}x_2}{\mathrm{d}t}\right), \quad (28)$$

where F_{coul1} and F_{coul2} are the Coulomb friction forces; k_{f1} and k_{f2} are the coefficients of viscous friction.

F_{01} and F_{12} are calculated by a dissipative contact force model (Machado et al., 2012; Ylinen et al., 2014) that contains a linear spring and a linear damper, as follows:

$$F_{01}=\begin{cases}K_{01}(x_1-x_{1max})+c_{01}\dfrac{\mathrm{d}x_1}{\mathrm{d}t}, & x_1>x_{1max},\\ K_{01}x_1+c_{01}\dfrac{\mathrm{d}x_1}{\mathrm{d}t}, & x_1<0,\end{cases} \quad (29)$$

$$F_{12}=\begin{cases}-K_{12}(x_{rel}-x_{12max})-c_{12}\left(\dfrac{\mathrm{d}x_2}{\mathrm{d}t}-\dfrac{\mathrm{d}x_1}{\mathrm{d}t}\right), & x_{rel}>x_{12max},\\ -K_{12}x_{rel}+c_{12}\left(\dfrac{\mathrm{d}x_1}{\mathrm{d}t}-\dfrac{\mathrm{d}x_2}{\mathrm{d}t}\right), & x_{rel}<0,\end{cases} \quad (30)$$

where K_{01} and K_{12} are the contact stiffnesses; c_{01} and c_{12} denote the damping coefficients; x_{12max} is the maximum of $x_{rel}=x_2-x_1$.

Through the dynamic analysis of the erecting beam and the load shown in Fig. 6, the expression of the external load F is derived (Wu et al., 2021) as follows:

$$F=\frac{J\varphi''+G\cdot l_g\cdot\cos(\varphi+\theta)\cdot l_{12}}{l_1\cdot l_2\cdot\sin(\varphi+\alpha)}, \quad (31)$$

where J is the moment of inertia of both the erecting beam and the load; φ'' is the angular acceleration. When the erecting beam is horizontal, the angle value of $\angle o_1 o o_2$ is α, and the angle between oo_g and the horizontal plane is θ. l_g, l_{12}, l_1, and l_2 are calculated by:

$$l_g = \sqrt{x_g^2 + y_g^2}, \tag{32}$$

$$l_{12} = \sqrt{\left(x_{o1} - x_{o2}\right)^2 + \left(y_{o1} - y_{o2}\right)^2}, \tag{33}$$

$$l_1 = \sqrt{x_{o1}^2 + y_{o1}^2}, \tag{34}$$

$$l_2 = \sqrt{x_{o2}^2 + y_{o2}^2}, \tag{35}$$

where x_{o1}, y_{o1}, x_{o2}, y_{o2}, x_g, and y_g are indicated in Fig. 6. Here, one absolute coordinate system (o-$x_o y_o$) is defined whose origin (o) is the hinge center between the erecting beam and bracket. The x-axis stays horizontal. x_{o1} and y_{o1} are coordinate values of the point o_1 that is the hinge point at the barrel end of the DATHC. x_{o2} and y_{o2} are the coordinates of the hinge point o_2 at the other end of the DATHC. x_g and y_g are the coordinates of the point o_g, the center of gravity of the load and the erecting beam.

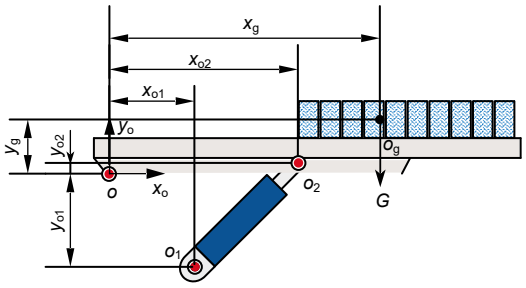

Fig. 6 Erecting beam and load

4 Results and discussion

4.1 Design constraint validation based on simulation

The simplified design constraint is an inequation involving λ in inequation (8). Therefore, first, the DATHC with different λ was simulated and verified. The crucial parameters of the system are shown in Table 1.

4.1.1 Effectiveness at different λ

In a horizontal state, the parameters of both the erecting beam and load, used to calculate F, are as shown in Table 2. The external load F at this point is marked $F1$.

In this study, 12 cases were simulated (Table 3). Note that the diameters conform to the China National Standard GB/T 2348 (SAMR, 2018). Moreover, all control signals were consistent in each case.

From Table 3, the top six cases did not meet the design constraint due to $\lambda > -1$. Their displacement curves are shown in Fig. 7. The left region denotes that the control signal for PDCV is positive, which means that DATHC is controlled to extend. The right region denotes that the control signal for PDCV is negative.

As expected, the speed was out of control in these six cases when the DATHC was retracted. Taking Case 1 as an example, we can obtain the velocity curve of the DATHC from Fig. 8a. v is the velocity of the DATHC. From 50 to 57.24 s (point A to B), the retraction speed of the DATHC is always maintained

Table 1 Crucial parameters of the system

Component	Parameter	Value
Motor	Rotary speed, n (r/min)	1500
Pump	Displacement, V (mL/r)	45
Relief valve	Cracking pressure, p_{k3} (MPa)	21
Proportional directional control valve	Flow rate at maximum opening (L/min)	100
Main valve of counterbalance valve	Setting pressure, p_{mk} (MPa)	21
	Pilot differential pressure for maximum opening (MPa)	0.7
	Pilot ratio, κ	3
	Characteristic flow rate at maximum opening (L/min)	60
Check valve of counterbalance valve	Cracking pressure, p_{ck} (MPa)	0.17
	Flow rate pressure gradient (L/(min·MPa))	450
DATHC	x_{1max} (mm)	911
	x_{12max} (mm)	848

Table 2 Parameters of erecting beam and load for $F1$

Parameter	Value
x_{o1} (mm)	800
y_{o1} (mm)	−961
x_{o2} (mm)	2000
y_{o2} (mm)	94
x_g (mm)	3346.52
y_g (mm)	458.82
G (N)	58 379.8

Table 3 Simulation cases with different λ

Case	d_1 (mm)	d_2 (mm)	d_3 (mm)	d_4 (mm)	λ
1	220	180	140	125	1.06
2	220	160	125	100	0.46
3	200	140	110	80	0.12
4	220	180	140	110	−0.23
5	220	200	140	120	−0.58
6	220	200	110	70	−0.94
7	220	200	125	80	−1.04
8	220	200	140	80	−1.25
9	220	200	160	100	−1.52
10	220	200	160	63	−1.69
11	200	180	160	80	−2.07
12	220	200	180	80	−2.37

at 0. However, from 50 s the signal to control retraction is given, and the DATHC is supposed to retract. Then, from 60 to 70.55 s (point *C* to *D*), its retraction speed varies from −0.021 to −0.024 m/s. Subsequently, the speed increases sharply, reaching −0.503 m/s at 74.69 s (point *E*). Following the accomplishment of switching stages at 76.56 s (point *F*), it is completely retracted at a speed of −0.026 m/s.

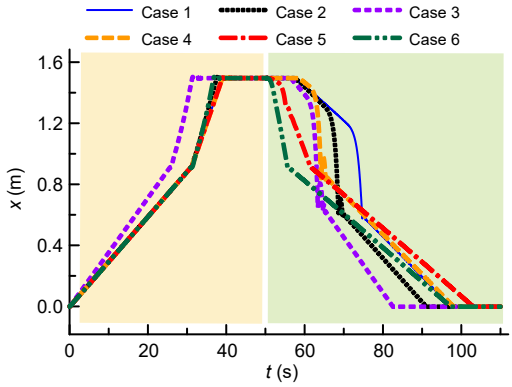

Fig. 7 Displacement curves of the DATHC in the first six cases

Case 6 had little effect on the displacement and velocity of the DATHC. This minor effect is difficult to observe from Figs. 7 and 8f, but the displacement curve of Stage 1 in Fig. 9 proves its existence. From 50 to 52 s, the displacement of Stage 1 changes slightly, but it is supposed to be standing still during this period. Because the value of λ in Case 6 is close to −1, the directions of the resultant forces on Stage 1

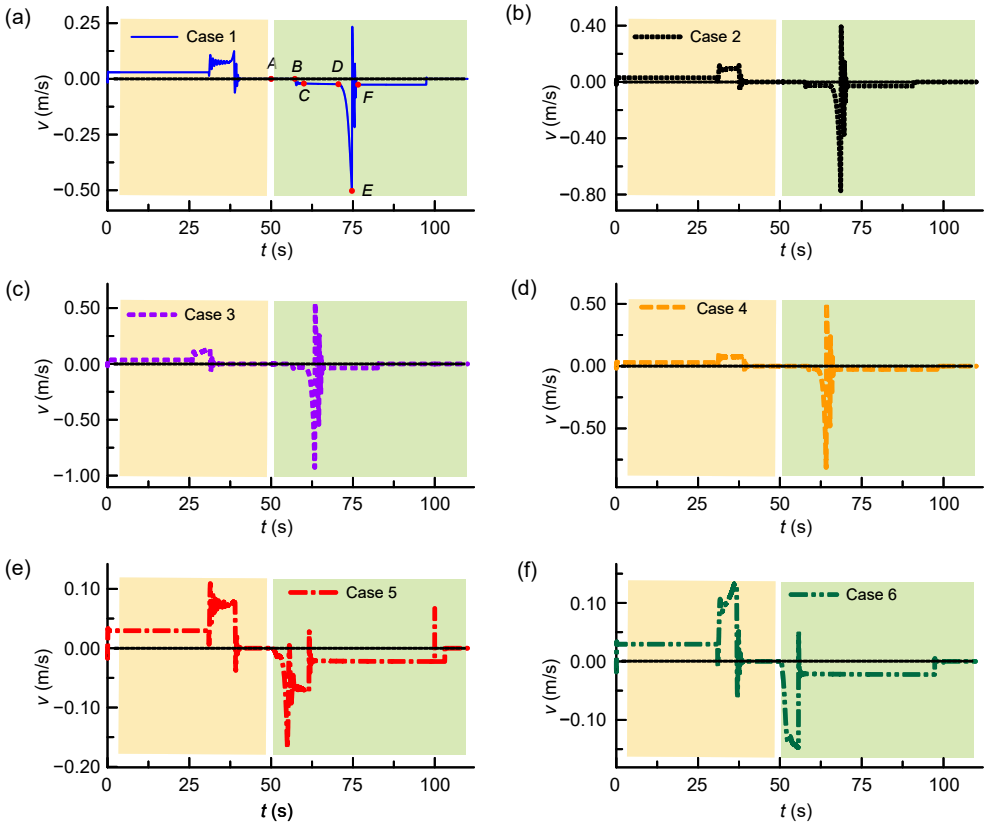

Fig. 8 Velocity curves of the DATHC in Cases 1–6 (a–f)

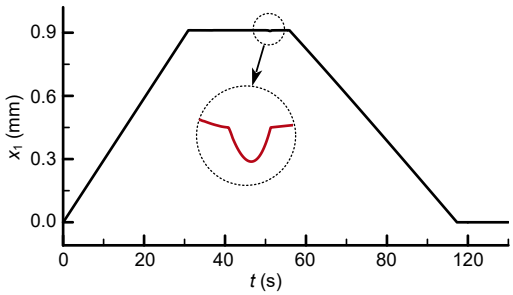

Fig. 9 Displacement curve of Stage 1 in Case 6

and Stage 2 easily change to correct directions. Moreover, the inertial forces and frictional forces are considered in the simulation, which are simplified or ignored in the derivation of design constraints. As a result, Case 6 had little effect on the performance of the DATHC.

The simulation results of the remaining six cases are shown in Figs. 10 and 11. Compared with Figs. 7 and 8, it is evident that the DATHC in the last six cases is able to extend and retract successfully. According to Fig. 11, from 50 s onwards, the DATHC begins to retract and a velocity step response occurs due to the step signal being inputted to the PDCV.

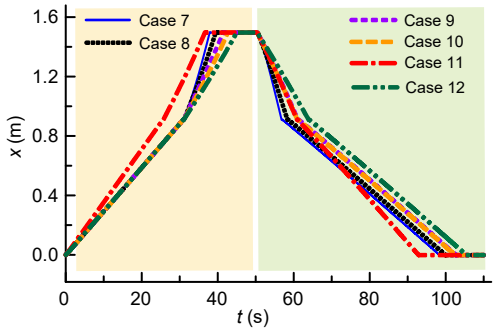

Fig. 10 Displacement curves of the DATHC in Cases 7–12

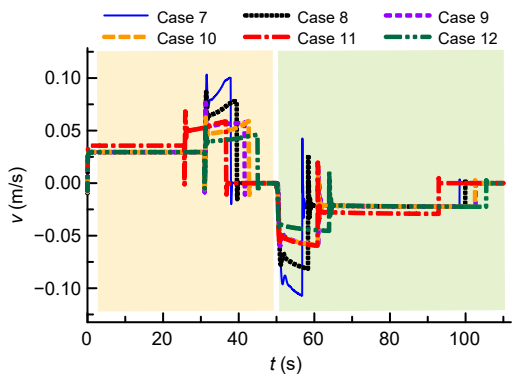

Fig. 11 Velocity curves of the DATHC in Cases 7–12

4.1.2 Effectiveness at different F values

The design constraint was proposed based on the DATHC force analysis, so it is necessary to conduct simulation and analysis on the DATHC under different values of F.

According to Eq. (31) and in consideration of the follow-up experiments, different F values were obtained by changing the parameters in Table 4. It should be emphasized that the coordinate values in Table 4 are those of the erecting beam in the horizontal position. Then, multiple sets of simulations were carried out by applying the different loads in Table 3 to Cases 1–12 in Table 3. Taking Cases 3 and 8 as random examples, from Figs. 12 and 13 we can see that the overspeed

Table 4 Different parameters for different F

F	x_{o1} (mm)	x_{o2} (mm)	x_g (mm)	y_g (mm)	G (N)
$F1$	800	2000	3346.52	458.82	5.84×10^4
$F2$	1000	2200	3313.14	507.95	1.17×10^5
$F3$	2200	1000	3313.14	507.95	1.17×10^5
$F4$	2400	1000	3313.14	507.95	1.17×10^5

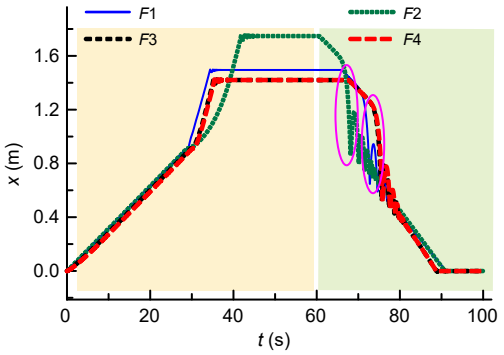

Fig. 12 Displacement curves of the DATHC in Case 3 with different loads

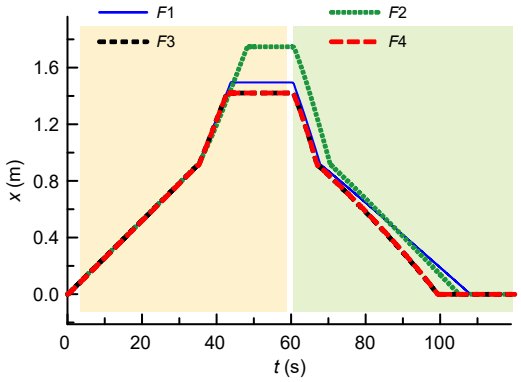

Fig. 13 Displacement curves of the DATHC in Case 8 with different loads

descent fault of the DATHC in Case 3 emerges under different loads as shown by the positions of the circles in Fig. 12, while that of Case 8 does not. Similar conclusions can be drawn from the rest of the cases. Therefore, the design constraint is still valid for different values of *F*.

4.2 Design constraint validation based on experiments

4.2.1 Experimental platform

To further verify the effectiveness of the design constraint, an erecting system experimental platform was built (Fig. 14). A schematic diagram of its hydraulic system is shown in Fig. 5. A displacement sensor was mounted on the DATHC to measure the displacement characteristics. The two ports of the DATHC and the "P" port of the PDCV were each equipped with a pressure sensor to obtain their dynamic pressure. A flow sensor was used to monitor the flow rate of the hydraulic pump to the DATHC. There are two ways to change the force acting on a DATHC. One is to change the number and installation positions of the load blocks installed on the erecting beam. The other is to adjust the position of the two hinged joints of the DATHC. In this way, the test rig was able to apply different loading forces on the DATHC (Table 4) to test the effectiveness of the design constraint under different *F* values.

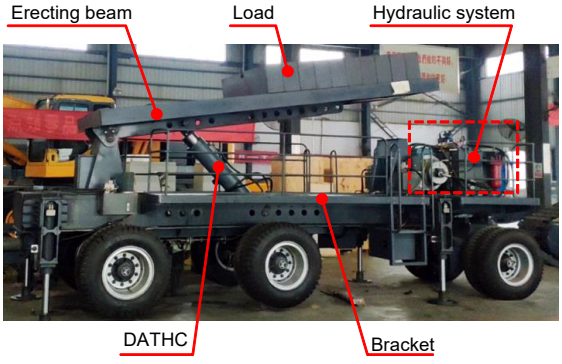

Fig. 14 Photo of the experimental platform

4.2.2 Experimental results

Because of the high manufacturing cost of the DATHC, only two cases were tested: one that met and one that did not meet the design constraint. As with the selection in Section 4.2.1, the two DATHCs were processed according to the parameters in Cases 3 and 8. Considering the damage caused by a possible drop for Case 3 not meeting the design constraint, Case 8 satisfying the design constraint was first tested under the heavy loads *F*2, *F*3, and *F*4 (Table 4). Case 3 was subsequently tested under the light load *F*1 (Table 4). Moreover, for the sake of reducing the swing of the erecting beam caused by pressure impact and collision during the experiments, the DATHC was slowed down in advance when it reached the switching stage position of the DATHC and the 90° position. This was done because the swing of the erecting beam could cause a greater inertia force due to the large moment of inertia which could affect the stability and safety of the experimental platform. In addition, the measured displacement signals were simply filtered for the convenience of subsequent comparison and analysis. The filtered displacement signals of the DATHC are shown in Figs. 15 and 16.

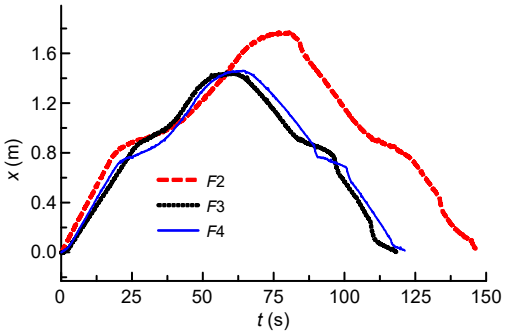

Fig. 15 Experimental displacement curves of the DATHC in Case 8

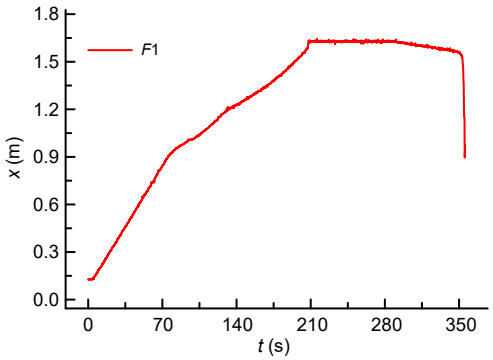

Fig. 16 Experimental displacement curve of the DATHC in Case 3

As is evident from Figs. 15 and 16, Case 8 still worked properly with different loads, whereas Case 3

experienced overspeed descent from 353.25 to 355.65 s, during which time the DATHC retracted 0.594 mm. These data indicate that the overspeed descent causes a rapid retraction only in Stage 2, which is consistent with the simulation results. After the occurrence of this fault, the experiment was terminated to avoid potential security hazards.

4.3 Further discussion

The above simulation and experimental results show that an overspeed descent fault of the erecting system will occur when the DATHC does not meet the design constraint. However, the mechanism of this fault is worth considering.

Using *F*1 in Case 3 as an example, the simulation displacement curves of Stage 1 and Stage 2 are shown in Fig. 17. A schematic diagram of the overspeed descent process is shown in Fig. 18. The blue arrows indicate the direction of movement.

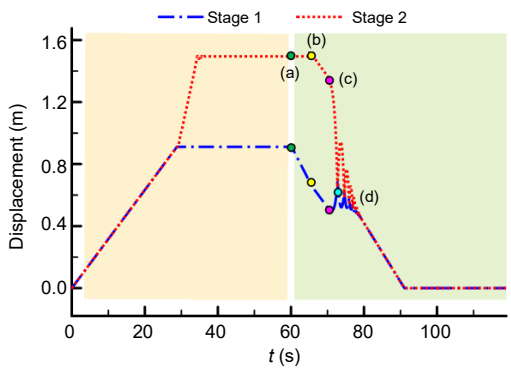

Fig. 17 Displacement curves of Stages 1 and 2 in Case 3

Firstly, because the diameters of the DATHC in Case 3 do not satisfy the design constraint, inequation (4) does not hold at the 90° position. According to the force analysis in Section 2.2, Stage 1 first retracts by resultant force, which corresponds to (a)–(b) in Figs. 17 and 18. During this period, the erecting beam does not rotate due to the static Stage 2.

Then, after Stage 1 retracts a certain distance, Stage 2 is pulled by Stage 1 and retracts in synchrony, as seen in Figs. 17 and 18 from (b) to (c). As the pulled Stage 2 retracts, the erecting beam is continuously lowered. At the same time, owing to the changing moment arm of the gravity *G*, the external load *F* acting on the DATHC gradually increases, varying from a pulling force (negative) to a pushing force (positive).

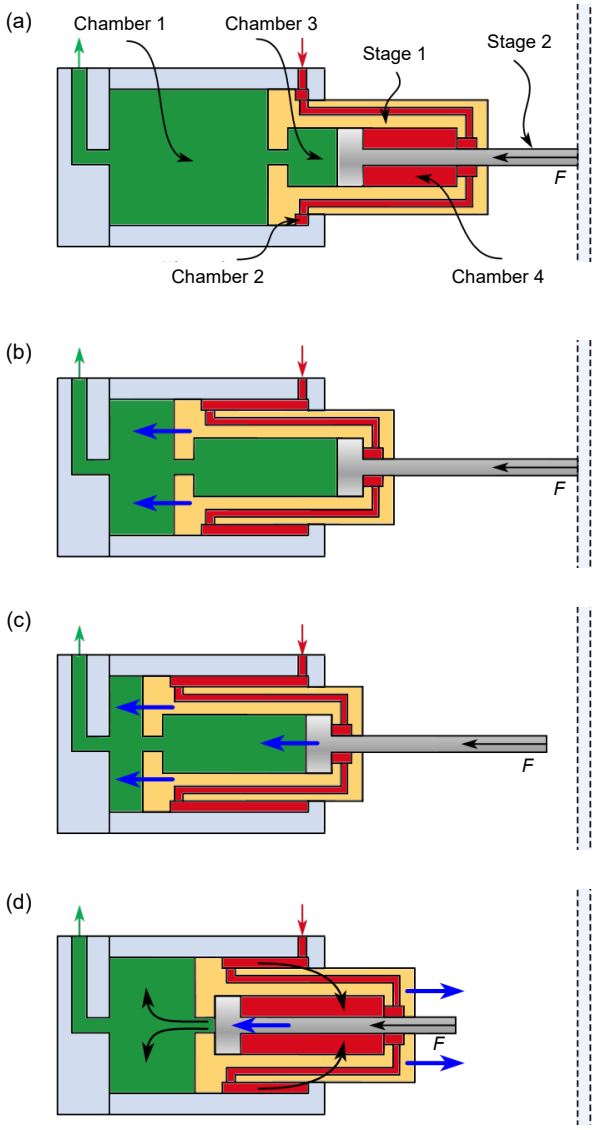

Fig. 18 Evolution of the fault of overspeed descent. (a)–(d) indicate the states of DATHC corresponding to (a)–(d) in Fig. 17. References to color refer to the online version of this figure

At some instant, the underlying inequation (4) starts to be true with increasing values of *F*, which means that the direction of the net force on Stage 1 changes. As a result, Stage 1 is required to extend to the maximum stroke position, as indicated in Figs. 17 and 18 from (c) to (d). With the extension of Stage 1, the volume of Chamber 1 increases, which causes oil in Chamber 3 to be sucked into Chamber 1, while oil from Chamber 2 is squeezed into Chamber 4. This process will accelerate the retraction of Stage 2, and in turn, the retraction of Stage 2 will promote the

extension of Stage 1. Because of this positive feedback loop, Stage 1 extends rapidly and Stage 2 quickly retracts, which leads to the overspeed descent of the erecting beam.

If the diameters of the DATHC meet the design constraint, then the underlying inequation (4) is always satisfied, and the above fault will not occur.

5 Conclusions

In this study, to avoid the overspeed descent fault of an erecting system caused by the improper design of a DATHC, a simplified design constraint was derived. After simplification, the design constraint related only to the diameters of the four effective areas of the DATHC, which makes the constraint easier to use for the design of DATHC. Then, multiple sets of simulations and experiments were performed to verify its effectiveness. The results showed that if the structural parameter of the DATHC, defined in Eq. (9), is less than −1, the erecting system will not have an overspeed descent fault. Moreover, the effectiveness was verified under different external loads. We also conclude that the design constraint is applicable not only when the DATHC is pushed and pulled during operation, but also when only a pushing or pulling force is applied to the DATHC.

When the design constraint is not satisfied, with increasing load force, the direction of the resultant force on Stage 1 changes during the retraction, then Stage 1 begins to extend while Stage 2 retracts. Since the two movements promote each other, the rate of descent goes out of control.

Acknowledgments

This work is supported by the National Natural Science Foundation of China (No. 91748210) and the National Outstanding Youth Science Foundation of China (No. 51922093).

Author contributions

Xiao-long ZHANG designed the research. Xiao-long ZHANG and Jun-hui ZHANG wrote the first draft of the manuscript. Shen ZHENG set up the test rig and processed the experiment data. Min CHENG helped organize the manuscript. Bing XU and Yu FANG revised and edited the final version.

Conflict of interest

Xiao-long ZHANG, Jun-hui ZHANG, Min CHENG, Shen ZHENG, Bing XU, and Yu FANG declare that they have no conflict of interest.

References

Bak MK, Hansen MR, 2013. Model based design optimization of operational reliability in offshore boom cranes. *International Journal of Fluid Power*, 14(3):53-65. https://doi.org/10.1080/14399776.2013.10801413

Cheng M, Xu B, Zhang JH, et al., 2017. Valve-based compensation for controllability improvement of the energy-saving electrohydraulic flow matching system. *Journal of Zhejiang University-SCIENCE A (Applied Physics & Engineering)*, 18(6):430-442. https://doi.org/10.1631/jzus.A1600346

Gao QH, 2004. Study on electrohydraulic proportion control in large-sized mechanism erecting process. *Chinese Journal of Mechanical Engineering*, 40(2):189-192 (in Chinese). https://doi.org/10.3321/j.issn:0577-6686.2004.02.042

Gupta SK, Prakash J, Kankar PK, 2020. Buckling load for telescopic cylinder using successive approximation method. *Indian Journal of Engineering and Materials Sciences (IJEMS)*, 27(4):853-859.

Hou JY, Zhang ZM, Ning DY, et al., 2017. Model-based position tracking control of a hose-connected hydraulic lifting system. *Flow Measurement and Instrumentation*, 53:286-292. https://doi.org/10.1016/j.flowmeasinst.2016.08.001

Lgritskaia A, Zabegaev A, Zverev V, et al., 2021. A method for reducing dynamic loads during switching stages of multistage hydraulic cylinders of launch vehicles rising drive. *AIP Conference Proceedings*, 2318:100013. https://doi.org/10.1063/5.0036242

Li CL, Su M, Xie ZP, 2015. Extreme research on the order motion of the hoisting two-stage hydraulic cylinder. *Applied Mechanics and Materials*, 727-728:430-434. https://doi.org/10.4028/www.scientific.net/amm.727-728.430

Lin TL, Lin YZ, Ren HL, et al., 2021. A double variable control load sensing system for electric hydraulic excavator. *Energy*, 223:119999. https://doi.org/10.1016/j.energy.2021.119999

Machado M, Moreira P, Flores P, et al., 2012. Compliant contact force models in multibody dynamics: evolution of the Hertz contact theory. *Mechanism and Machine Theory*, 53:99-121. https://doi.org/10.1016/j.mechmachtheory.2012.02.010

Park CG, Yoo S, Ahn H, et al., 2020. A coupled hydraulic and mechanical system simulation for hydraulic excavators. *Proceedings of the Institution of Mechanical Engineers, Part I: Journal of Systems and Control Engineering*, 234(4):527-549. https://doi.org/10.1177/0959651819861612

Prakash J, Gupta SK, Kankar PK, 2020. An analytical approach to evaluate the maximum load carrying capacity for pin-mounted telescopic hydraulic cylinder. *Proceedings of the Institution of Mechanical Engineers, Part C: Journal of Mechanical Engineering Science*, 234(19):3919-3934. https://doi.org/10.1177/0954406220916524

Ritelli GF, Vacca A, 2013. Energetic and dynamic impact of counterbalance valves in fluid power machines. *Energy Conversion and Management*, 76:701-711.

https://doi.org/10.1016/j.enconman.2013.08.021

SAMR (State Administration for Market Regulation), 2018. Fluid Power Systems and Components—Cylinder Bores and Piston Rod Diameters, GB/T 2348-2018. Standardization Administration, Beijing, China (in Chinese).

Tran XB, Hafizah N, Yanada H, 2012. Modeling of dynamic friction behaviors of hydraulic cylinders. *Mechatronics*, 22(1):65-75. https://doi.org/10.1016/j.mechatronics.2011.11.009

Uzny S, Kutrowski Ł, 2019. Strength analysis of a telescopic hydraulic cylinder elastically mounted on both ends. *Journal of Applied Mathematics and Computational Mechanics*, 18(1):89-96. https://doi.org/10.17512/jamcm.2019.1.08

Wang XW, Yang ZJ, Feng JL, et al., 2013. Stress analysis and stability analysis on doubly-telescopic prop of hydraulic support. *Engineering Failure Analysis*, 32: 274-282. https://doi.org/10.1016/j.engfailanal.2013.04.006

Wu QP, Ma C, Li L, et al., 2021. Load simulation analysis of a new erection system based on the gas-assisted drive erecting scheme. *Journal of Physics: Conference Series*, 1750:012039. https://doi.org/10.1088/1742-6596/1750/1/012039

Xie Z, Xie J, Du WZ, et al., 2014. Time-varying integral adaptive sliding mode control for the large erecting system. *Mathematical Problems in Engineering*, 2014:950768. https://doi.org/10.1155/2014/950768

Yanada H, Sekikawa Y, 2008. Modeling of dynamic behaviors of friction. *Mechatronics*, 18(7):330-339. https://doi.org/10.1016/j.mechatronics.2008.02.002

Yang J, Huang SZ, Zeng L, 2019. Robust switched control strategy of large erecting equipment hydraulic systems. *China Mechanical Engineering*, 30(22):2698-2703 (in Chinese). https://doi.org/10.3969/j.issn.1004-132X.2019.22.008

Ylinen A, Marjamäki H, Mäkinen J, 2014. A hydraulic cylinder model for multibody simulations. *Computers & Structures*, 138:62-72. https://doi.org/10.1016/j.compstruc.2014.02.006

Zhou H, Hou JY, Zhao YG, et al., 2012. Model-based trajectory tracking control for an electrohydraulic lifting system with valve compensation strategy. *Journal of Central South University*, 19(11):3110-3117. https://doi.org/10.1007/s11771-012-1386-6